Effect of liquid viscosity on the aerodynamic breakup of non-spherical droplets

Konstantinos Bergeles[1,*], Georgios Charalampous[1], Yannis Hardalupas[1] and Alex M. Taylor[1]
[1]Mechanical Engineering Department, Imperial College London, UK
*Corresponding author: k.bergeles12@imperial.ac.uk

Abstract

This paper studies the effect of liquid viscosity on the atomisation regimes of initially spherical and non-spherical droplets and also kinematic characteristics of non-spherical droplets. The droplets consisted of water-glycerol solutions with viscosities ranging from 6.3 to 697 mPa s, and the initial aspect ratio was 1<AR<2. The range of We number was from 10 to 200 and of the Oh number from 0.01 to approximately 4. The experimental findings showed that the equivalent We_{eq} and Oh_{eq} numbers, proposed in previous work [1] for water droplets, are also applicable to spherical and non-spherical droplets in the range of Oh numbers of this study in order to classify the breakup regimes on the existing morphological charts. The kinematic characteristics of the centre of mass for droplets with AR=1.2 are evaluated and the role of viscosity examined in the no breakup and bag-stamen regimes.

Keywords

non-spherical, droplet, breakup, aerodynamic

Introduction

Understanding the physics and nature of liquid droplet-air interaction, investigating the droplet internal and external flow and capturing droplet deformation and breakup is of importance in various scientific fields and technological applications [2]. In some technological applications, such as automotive sprays, the need is to avoid the generation of the largest droplets. Although their number density is low, these sizes carry a disproportionate fraction of the injected fuel, which evaporates slowly, and follow 'ballistic' trajectories resulting in locally overly rich mixtures, associated with undesirable emission characteristics.

The literature on experimental droplet atomisation assumes an initial spherical droplet. In other words, most research classifies and investigates the breakup modes under morphological regimes treating the droplet as a sphere. However, in regions of intense atomisation, as found in the interior of the crankcase, the technological motivator of the present work, droplets are known to have an initial non-spherical shape before the interaction with the flow inside the crankcase.

According to Hinze[3] droplets droplet deformation occurs as the value of We becomes greater than one (We >1). The external aerodynamic force acting on the droplet's surface, which scales as ρu^2 becomes larger than the counteracting force owing to the surface tension σ/d_0 of the liquid. The deformation evolves to breakup at the critical value of We_{crit}=12 number. In cases where $We \approx We_{crit}$ number simple breakup mechanism occurs, while for increasing We number, the disintegration of the droplet becomes a more chaotic atomisation process.

Pilch and Erdman[4] performed experiments to quantify characteristic variables of the breakup process, classifying the breakup modes. For increasing We number the atomisation regimes found were the vibrational, bag, bag-stamen, sheet stripping and catastrophic breakup as shown in Figure 1. The normalised displacement x_{d*} (Eq. (1)), velocity u_d^* (Eq. (2)) and acceleration a_d^* (Eq. (3)) of the centre of mass of the droplet were also presented. The study modelled the droplet as a rigid sphere, neglecting mass loss during the atomisation, as also the droplet velocity relative to the flow assuming an average, constant drag coefficient C_d throughout the breakup process.

$$x_d^* = \frac{x_d}{d_0} = \frac{3}{8}\,C_d\,(t^*)^2 \tag{1}$$

$$u_d^* = \frac{u_d}{u_g \cdot \epsilon^{0.5}} = \frac{3}{4}\,C_d\,t^* \tag{2}$$

$$\alpha_d^* = \frac{\alpha_d \cdot d_0}{u_g^2 \cdot \epsilon} = \frac{3}{4}\,C_d \tag{3}$$

, where x_d, u_d, a_d are the dimensioned displacement, velocity and acceleration of the centre of mass of the droplet. The timescale t^* of the atomisation phenomenon (Eq. (4)) equals to:

$$t^* = \frac{t \cdot u_g\,\epsilon^{1/2}}{d_0}, \tag{4}$$

where ϵ is the density ratio ρ_g/ρ_l, t is the dimensioned time and C_d is the droplet drag coefficient which remains constant during the atomisation and equal to $C_d = 2.5$ and $C_d = 1.7$ for compressible and incompressible flows respectively.
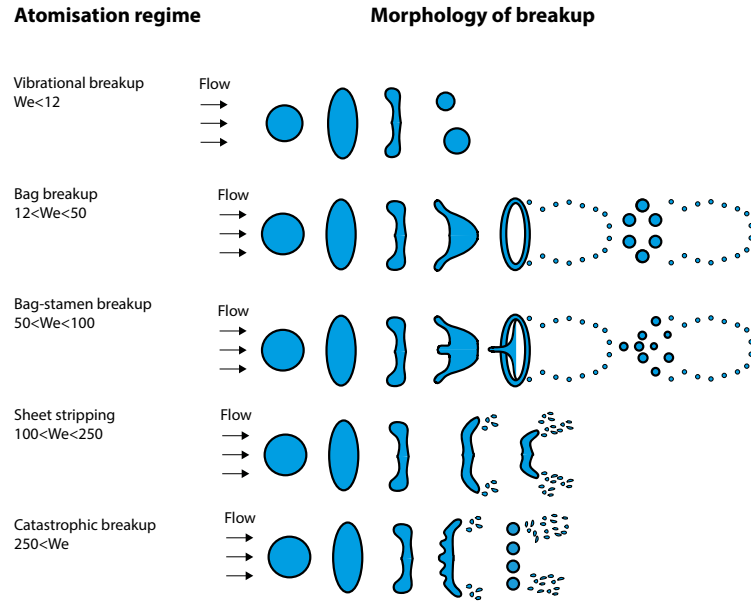
Atomisation regime   **Morphology of breakup**

Figure 1. Morphological classification of breakup modes based on We number as derived by Pilch and Erdman [4]

In addition Pilch and Erdman [4] proposed a third degree polynomial to express the droplet displacement x_{d*} (Eq. (5)), velocity u_d^* (Eq. (6)) and acceleration a_d^* (Eq. (7)) using the empirical constant B to provide a correct initial behaviour.

$$x_d^* = \frac{x_d}{d_0} = \frac{3}{8} C_d \left(t^*\right)^2 + B \left(t^*\right)^3 \tag{5}$$

$$u_d^* = \frac{u_d}{u_g \cdot \epsilon^{0.5}} = \frac{3}{4} C_d \, t^* + 3B \left(t^*\right)^2 \tag{6}$$

$$\alpha_d^* = \frac{\alpha_d \cdot d_0}{u_g^2 \cdot \epsilon} = \frac{3}{4} C_d + 6B \, t^* \tag{7}$$

with C_d=1, B=0.116 for compressible flow and C_d=0.5, B=0.0758 for incompressible flow. The correlation assumes a constant drag coefficient C_d of a rigid constant-mass sphere. the change of the frontal area of the droplet due to deformation is not taken into account. Moreover, the equations are valid for the period of time until the velocity of the droplet is 60% of the velocity of the flow.

The transition between two breakup regimes has been found to be a function of the We and Oh number and independent of the density ratio or the Re number. These transitional We numbers have been quantified by Brodkey [5] in Eq. (8) and Gelfand [6] in Eq. (9).

$$We_{\mathrm{crit}} = We_{\mathrm{crit},0} \left(1 + 1.077 \, Oh^{1.6}\right) \tag{8}$$

$$We_{\mathrm{crit}} = We_{\mathrm{crit},0} \left(1 + 1.5 \, Oh^{0.74}\right) \tag{9}$$

, where We_{crit} is the transitional We number for increased Oh number and $We_{\mathrm{crit},0}$ is the transitional We number for $Oh \to 0$ respectively.

However a gap exists in the literature of the droplet atomisation as all the previous analytical work and interpretation of experimental data assumed initial spherical droplets.

Experimental arrangement and measurement technique

The experimental arrangement is shown in Figure 2. The main components are a Tec5 ultrasonic levitator which is used to levitate individual droplets and control their sphericity, a Photron CMOS high-speed camera for the imaging of the breakup and a nozzle controlled by a high-speed solenoid valve which produces the cross-flow that atomises the droplet.

Droplet levitation: An ultrasonic wave is emitted from the transducer of the levitator, which is reflected back to its source by a reflector, creating a vertical standing wave. A single droplet with diameter of the order of one millimetre is
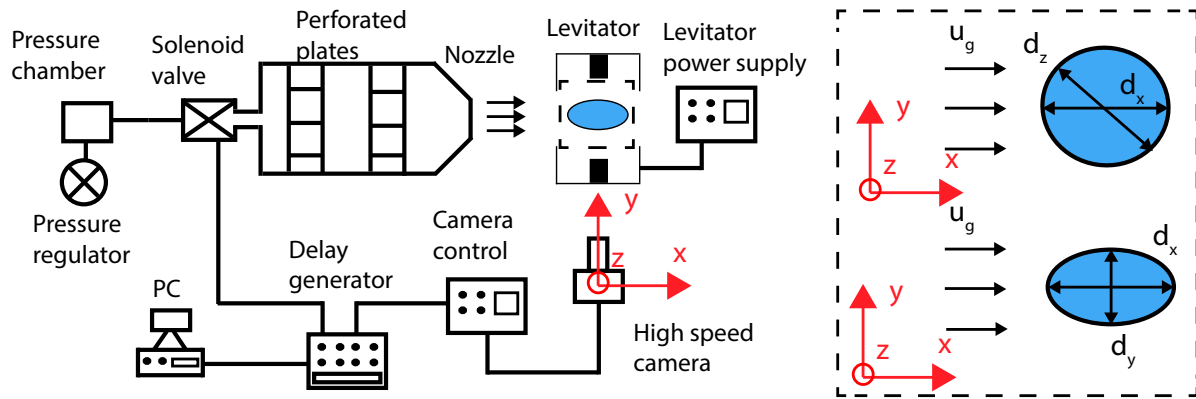
Figure 2. Experimental arrangement of the aerodynamic breakup study of spherical and non-spherical droplets

Table 1. Physical properties of glycerol-water solutions at 20°C ambient temperature

Name (% glycerol)	Dynamic viscosity μ_l [mPa s]	Kinematic viscosity ν_l [mm^2/s]	Density ρ_l [kg/m^3]	Surface tension σ [mN/m]
Mix-1 (50%)	6.386	5.674	1125.5	68.5
Mix-2 (80%)	58.96	48.839	1207.3	65.5
Mix-3 (97%)	697	557.15	1251.0	63.0

placed at a pressure node and levitated until aerodynamically atomised from a high speed air stream. The sphericity of the droplet is controlled by adjusting the amplitude of the ultrasonic waves, permitting the transformation of a spherical droplet into an oblate spheroidal droplet.

The acoustic pressure induced on the upper and lower pole of the droplet plays a minor role during the deformation and atomisation process. For a millimetre droplet, the lift force generated by the acoustic pressure balances the gravitational force and caused a total pressure within the droplet to increase by approximately 10 Pa. The acoustic pressure is the cause of transformation of the spherical droplet shape into an oblate spheroidal shape, due to surface tension, approximately 70 Pa for the maximum AR. The minimum dynamic pressure of the flow is 500 Pa, therefore the contribution of the maximum acoustic pressure to the droplet atomisation is an order of magnitude lower compared to the minimum dynamic pressure of the flow. As a result, the role of the acoustic pressure on the atomisation is expected to be negligible.

Gas flow: The droplets were impulsively accelerated by a sudden gust of air, which was released from a pressure chamber by a fast solenoid valve. The cross-flow consisted of filtered air at room temperature $20°$ C. The air jet flow was ejected through a nozzle with 10mm diameter. The velocity at the exit of the nozzle was measured using a Dantec hotwire device to examine the uniformity and repeatability of the velocity profile. The velocity profile of the flow as a function of time is close to a step function with accelerations ranging from 1928 up to $13 \cdot 10^3$ m/s^2 over the range of experiments. The coefficient of variance of the acceleration is lower than 8% for all operating conditions.

The maximum and mean velocity value of the flow were measured at four distinct points at a radius of 2mm and at the centre of the nozzle. The measurements, show an almost uniform velocity profile with a standard deviation well below 3%, thus the droplet atomisation occurs under a uniform velocity profile. However, for low air velocities, discrepancies in the flow are larger, but still within an acceptable range with maximum standard deviation of around 4.3 %.

High-speed imaging: The shadowgraphic technique is employed for the visualisation of the droplet breakup. A Photron high-speed CMOS camera records the droplet breakup at a frame rate of 20 kHz. The spatial resolution of the images is 512 x 256 pixels with 5μs exposure time. A commercial Nikon lens (f-number f/#=2.8) with appropriate extension tubes and a teleconverter (TELEPLUS MC7 AF 2.0X DGX) are used leading to an image magnification of 12.3 μm/pixel. The imaged area of the camera is 6.2mm x 3.1mm in the xy plane as shown in Figure 2.

Due to the high acquisition rate, the droplet breakup was temporally resolved. The camera was placed perpendicular to the flow direction and it was focused on the symmetry plane of the droplet. The synchronisation of the solenoid valve with the high-speed camera was achieved using a SRS 535 digital delay generator. Finally, a back illumination lamp of 1000 W was used and uniform illumination was accomplished with ground glass diffusers. The processing of the images was performed in Matlab environment using an in-house code and in ImageJ [7], an image manipulation software.

For the present study three glycerol-water solutions were produced and the viscosity measured using a viscometer. The physical properties were derived for 20°C ambient temperature and the characterisation error is within 2%. Table 1 summarises the physical properties of the glycerol-water solutions.

Morphological classification of droplet breakup

The breakup modes appearing for increasing We numbers are the no, bag, bag-stamen and sheet stripping breakup modes. These regimes change for increasing Oh numbers and it must be pointed out that the transition between breakup regimes is not a step function but it occurs gradually. Therefore the characterisation of a breakup could be difficult and rather arbitrary, especially between bag-stamen and sheet stripping breakup regimes and also for viscous liquids.

The most commonly used theoretical curves describing this transition of the breakup modes are produced by Brodkey [5] (Eq. (8)) and Gelfand [6] (Eq. (9)). According to these relations, a steep change in the transitional We numbers appears for higher Oh number ($Oh > 0.1$). From this Oh number and onward the liquid viscous forces become dominant and an exponential change occurs to the transitional We numbers.

The morphological classification in the Oh - We number plane of the present experimental data is shown in Figure 3. The derivation of the dimensionless numbers was done with the diameter d_0 based on droplet's volume. Overlapping regions appeared, especially in the bag and bag-stamen breakup regimes for Mix-1 (50% glycerol) and Mix-2 (80% glycerol) solutions.

The theoretical curve of Brodkey [5] and Gelfand [6] are also presented in Figure 3. The regime boundaries are approximately flat for $Oh < 0.1$; Gelfand's relation [6] produces higher transitional We numbers for lower Oh numbers than Brodkey's [5] , however the latter one predicts a steeper change in the transitional We numbers. The theoretical curves of Brodkey [5] and Gelfand [6] predicting the breakup regime boundaries should be taken as a general rule.

For $Oh > 0.05$ the discrepancies of the two theoretical curves become significant, showing that the transition criteria of breakup regimes for increasing Oh are not well defined even for initially spherical droplets. The experimental data does not agree with the predicted transitional We numbers because the initial sphericity of the droplet has not taken into consideration by the theoretical curves.

Figure 4 is the representation of the breakup modes in We_{eq} - Oh_{eq} plane. The derivation of the dimensionless numbers was done with the equivalent droplet diameter d_{eq} (Eq. (11). The equivalent We_{eq} [1] (Eq. (10)) number for deformed droplet is:

$$We_{eq} = \frac{\rho_g \, u_g^2 \, d_{eq}}{\sigma} \tag{10}$$

, where d_{eq} is the equivalent diameter and defined in Eq. (11)

$$d_{eq} = \frac{d_x^2}{d_y} \tag{11}$$

, where d_x, d_y are the stream-wise and cross-stream diameter of the droplet respectively. In the case of the spherical droplet, the equivalent diameter is equal to the diameter of the droplet d_0 based on its volume. In the same way the equivalent Oh_{eq} [1] is formulated (Eq. (12))

$$Oh_{eq} = \frac{\mu_l}{\sqrt{\rho_l \, \sigma \, d_{eq}}} \tag{12}$$

Figure 3 and Figure 4 map the breakup mode of both initially spherical and non-spherical droplets; however the initial sphericity of the droplets is not illustrated in the figures for clarity purposes. The introduction of d_{eq} to the Oh number gives $Oh_{eq} < Oh$; in other words the equivalent diameter d_{eq} "reduces" the effect of liquid viscosity (and as a consequence of the overall Oh number) to the transition of breakup modes. For the same We number, higher initial d_{eq} leads to lower Oh_{eq} compared to a spherical droplet (d_0, Oh) resulting to a "higher" breakup regime. The combined effect of the equivalent Oh_{eq} and We_{eq} is to translate the experimental data upwards and to the left; meaning that if one is held constant the introduction of d_{eq} leads to "higher" breakup regimes.

For the two least viscous solutions (50% and 80% glycerol) the overlapping of the experiential data appears decreased compared to the We-Oh plane representation. Additionally, both sets of experimental data are in better agreement with the two theoretical curves (Figure 8 and Figure 9).

The equivalent dimensionless groups (We_{eq} and Oh_{eq}) incorporate the initial non-sphericity of the droplets which lead to a better mapping of the experimental data than the conventional We and Oh numbers. For droplets with $Oh > 1$ (97% glycerol) the regions where breakup modes overlap remains. As the viscosity effects become dominant, the role of Oh number becomes important.

Effect of liquid viscosity to the kinematic characteristics of droplets

The displacement x_d^*, velocity u_d^* and acceleration α_d^* of the centre of droplet's viewable area are presented as a function of dimensionless time t^* for water and three glycerol-water solutions (50%, 80% and 97% glycerol). The results of the study are split in two sections, for low and high We numbers, or in other words for no and bag-stamen breakup regimes. The aspect ratio AR chosen for this study is $AR =1.2$. It could be achieved with all liquid with satisfactory repeatability leading to minimisation of the errors regarding the droplet's volume and initial AR; both of the errors are below 5%. For the normalisation of the results the diameter d_0 is used. This is done in order to maintain the physical meaning of the kinematic characteristics. For example, an initially spherical droplet translates faster than an initially non-spherical. When d_{eq} is employed for the normalisation of the velocity this would not be the case for the non-dimensional velocity u_d^*. However, in the present paper, since the is constant ($AR =1.2$), diameter d_{eq} could be used as well as it is the same for all breakup cases presented.
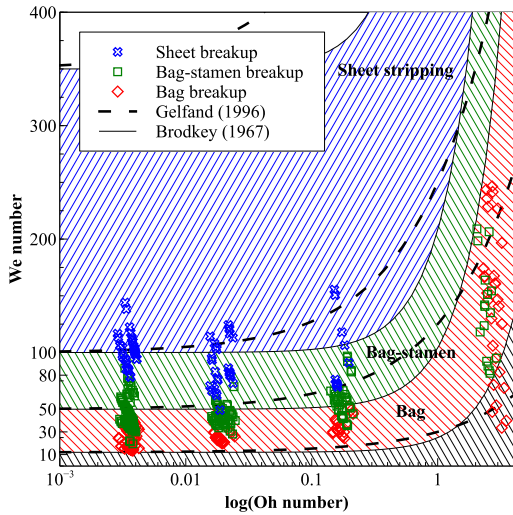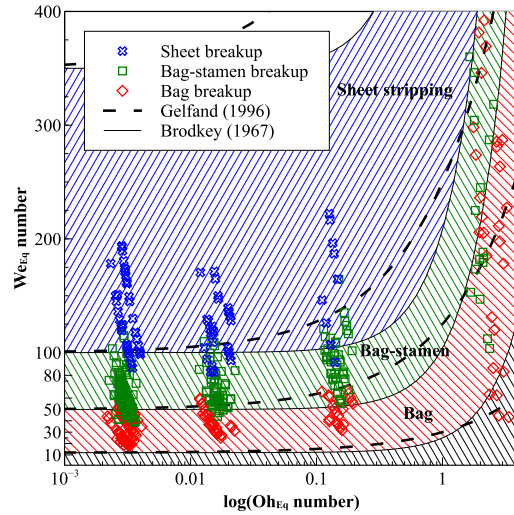
Figure 3. Morphological classification of breakup modes of spherical and non-spherical droplets consist of water and *Mix*-1, 2 and 3 (50%, 80% and 97% glycerol) in We-Oh plane derived with d_0

Figure 4. Morphological classification of breakup modes of spherical and non-spherical droplets consist of water and *Mix*-1, 2 and 3 (50%, 80% and 97% glycerol) in We_{eq}-Oh_{eq} plane derived with d_{eq}

Low We number - No breakup regime

The We number ranges from 10 to 13 with the Oh number being $3.4\,10^{-3}$, 0.02, 0.19 and 2.2 for increasing liquid viscosities. The diameter d_0 based on the droplet volume is d_0 =1.25$\pm$0.05mm and the AR =1.20$\pm$0.02 The variation in the values for We number occurs due to the difference in the physical properties of the liquids, namely the density and the surface tension.

Figure 5a presents a comparison of the non-dimensional displacement x_d^* of the centre of viewable area of the droplet with dimensionless time t^* for the four liquids (water and 50%, 80% and 97% glycerol) with the 3rd degree fitting curve of Pilch and Erdman [4] which is independent of viscosity. The fitting curve generally under-predicts the displacement of the droplet and this is mainly due to the increased frontal area of the droplets compared to the spherical droplet assumed by the 3rd degree fitting curve.

Figure 5b shows the non-dimensional velocity u_d^* of the centre of viewable area of the droplet. For glycerol-water solutions, after they achieve their maximum deformation d_{max}^*, which occurs at t_{max}^*=1.18, 2.55 and 2.6 for 50%, 80% and 97% glycerol solutions respectively, they continue to translate with constant frontal area approximately equal to their maximum deformation.

Regarding the water droplet, its velocity u_d^* oscillates due to the changes of the frontal area of the droplet. At t_{max}^*=1.07 the water droplet achieves its maximum deformation d_{max}^*=1.42, however at t^*=2.1 it becomes nearly spherical again. The reason why the oscillatory behaviour did not appear to that extent for the glycerol-water solutions is because the increased viscosity dampens the droplet oscillations. This oscillatory behaviour is not predicted by the 3rd degree fitting curve. The velocities of the droplet as they exit the imaged area are u_d^*=2.6, 2.8, 3.3 and 3.0 for increasing liquid viscosity and are directly related to the droplet frontal area.

The extent of the droplet's oscillatory behaviour decreases with the increase of the liquid viscosity as also does its effect on the translation behaviour of the droplet. Figure 5c shows the temporal evolution of the normalised acceleration of the droplet α_d^*. The data for the acceleration were derived by fitting a 5th degree polynomial to the displacement data of the four liquids and taking the second derivative of the polynomial. A 5th degree polynomial was used so that its second derivation was a third degree, which is able to predict the oscillation; the correlation coefficient is more than 0.95 regarding the displacement data. The bars in Figure 5c indicate the difference of the fitting curve value from the corresponding value of the experimental data for the acceleration α_d.

The acceleration provides an overview of the behaviour of the droplet's frontal area with time; in particular the rate of change of the acceleration is related with the rate of change of the frontal area. As expected the water droplet accelerates faster than the rest of the droplets as it deforms faster due to its low viscosity. Additionally, the water and the least viscous glycerol-water solution (50% glycerol) are oscillating; Mix-2 (80% glycerol) oscillates but with a very small amplitude and finally no oscillation occurs for the most viscous case (97% glycerol). The two least viscous droplets accelerate faster than the other two more viscous droplets. After that time the frontal area of the two droplet reduces and therefore the acceleration decreases; at time t^*=1.6 the two more viscous droplets, which did not oscillate, have higher acceleration than the least viscous droplets despite the fact that the latter ones have higher rate of increase of the frontal area.
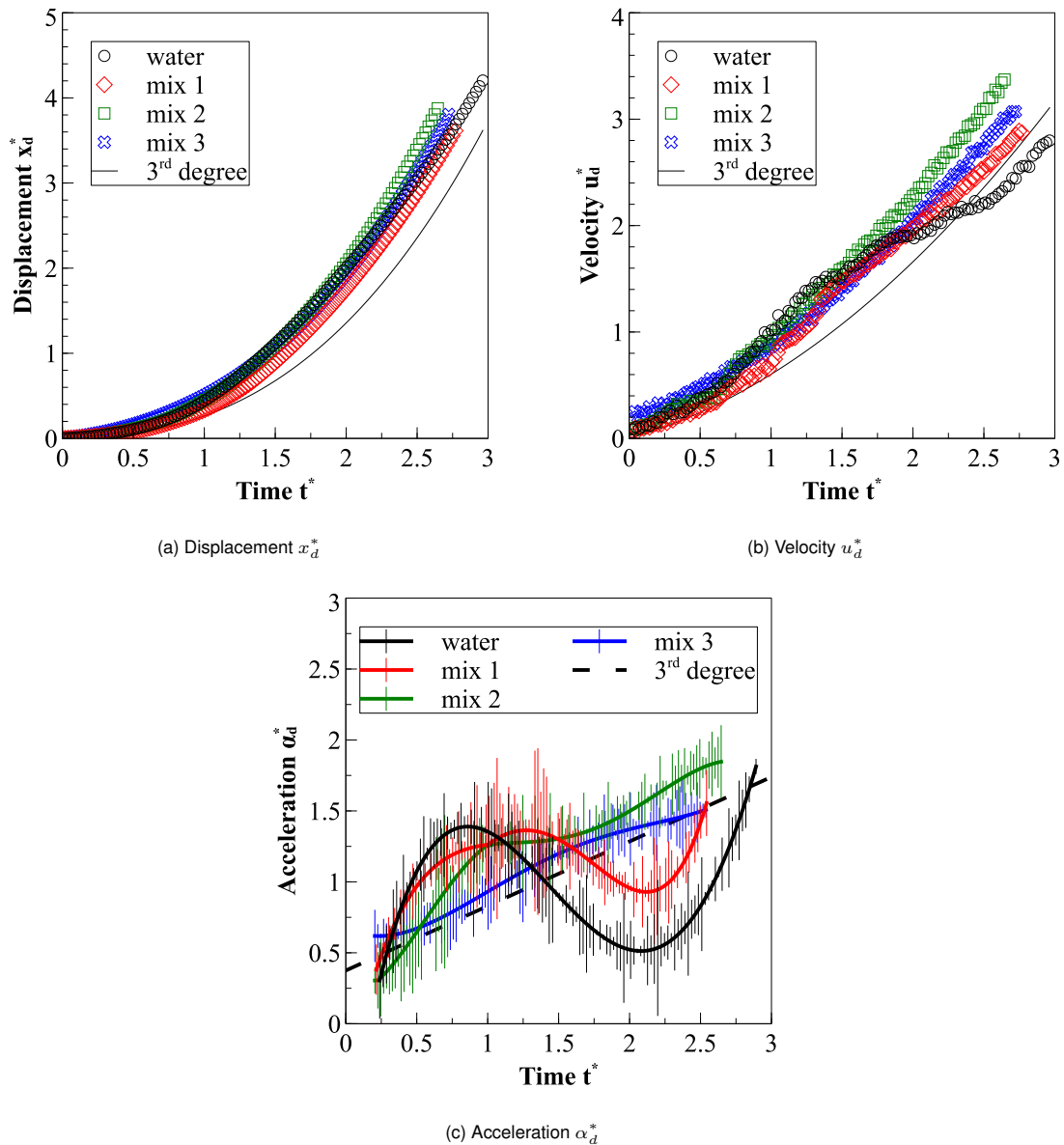
(a) Displacement x_d^*

(b) Velocity u_d^*

(c) Acceleration α_d^*

Figure 5. Comparison of the temporal evolution of the **(a)** displacement x_d^*, **(b)** velocity u_d^* and **(c)** acceleration α_d^* of oblate droplets (AR=1.2) under the *no* breakup regime for water, 50%, 80% and 97% glycerol solutions with the 3rd degree fitting curve
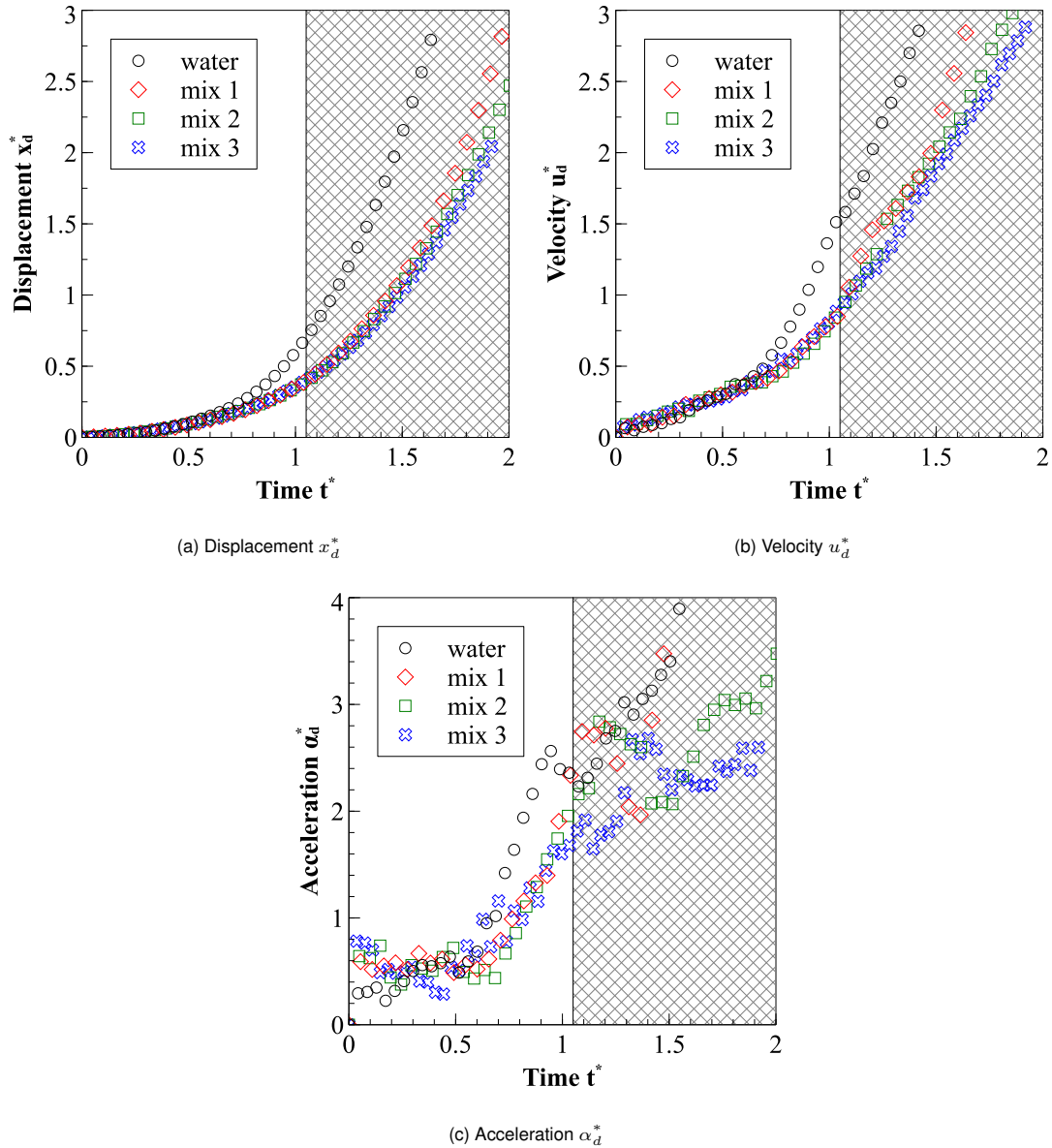[4]

(a) Displacement x_d^*

(b) Velocity u_d^*

(c) Acceleration α_d^*

Figure 6. Comparison of the temporal evolution of the **(a)** displacement x_d^*, **(b)** velocity u_d^* and **(c)** acceleration α_d^* of the centre of mass of oblate droplets (AR=1.2) under the *bag-stamen* breakup regime for water, 50%, 80% and 97% glycerol solutions with the 3rd degree fitting curve [4]

High We number - Bag-stamen breakup regime

Figure 6 presents the measured displacement x_d^*, and the deduced velocity u_d^* and acceleration α_d^* of the droplet centre of mass with time for various liquid viscosities. The gray area of the figures correspond to the breakup initiation time t_{init}^* of the most viscous case and is equal to t_{init}^* =1.02; the corresponding breakup initiation time for the least viscous droplet is t_{init}^* =0.97.

At short times the effect of increasing viscosity on both displacement and velocity is minor, despite the order of magnitude in the viscosity differences. Detailed differences can be seen in the acceleration values (Figure 6c). The acceleration of the water droplet at time t^*=0 is smaller than the acceleration for the more viscous droplet due to the higher initial deformation. In later times, due to its higher frontal area the acceleration increases and consequently its velocity increases and its displacement overtake the other droplets. It is of interest to notice that the three more viscous cases have almost the same velocity and displacement and trajectory differentiation starts much latter in time, in fact approximately around the breakup initiation time.

Conclusions

The role of the initial sphericity of the droplet on the breakup process was experimentally investigated, over a range of We from 10 to 200 and of the Oh number from 0.01 to approximately 4. It was observed that the breakup modes of initially spherical droplets were in good agreement with the literature but equivalent We_{eq} and Oh_{eq} numbers were required to extend the existing morphological classification charts for initially non-spherical as well as spherical

droplets. For the higher Oh numbers (Oh>1) not a discernible distinction between breakup modes was possible. The kinematic characteristics of droplets of AR=1.2 showed that the liquid viscosity has an important role through the dampening of the internal flow field and two viscosity droplets are accelerated at higher rates due to faster deformation which results in greater frontal area.

Acknowledgments

Nomenclature

t	time [s]
t^*	dimensionless time [-]
AR	aspect ratio [-]
We	Weber number [-]
We_{eq}	equivalent Weber number [-]
Oh	Ohnesorge number [-]
Oh_{eq}	equivalent Ohnesorge number [-]
$\rho_{g,l}$	gas, liquid density [kg/m^3]
u_g	gas velocity [m/s]
d_0	volume based droplet diameter [m]
d_{eq}	equivalent droplet diameter [m]
$\mu_{g,l}$	gas liquid dynamic viscosity [Pa s]
σ	surface tension [N/m]
ϵ	density ratio [-]
C_d	drag coefficient [-]
x_d^*	dimensionless droplet displacement [-]
u_d^*	dimensionless droplet velocity [-]
α_d^*	dimensionless droplet acceleration [-]

References

[1] K. Bergeles, G. Charalampous, Y. Hardalupas, and A. M. K. P. Taylor, "Breakup of Non-spherical Droplets," in *27th Annual Conference on Liquid Atomization and Spray Systems*, vol. 1, pp. 4–7, 2016.

[2] E. Villermaux, "Fragmentation," *Annual Review of Fluid Mechanics*, vol. 39, pp. 419–446, jan 2007.

[3] J. O. Hinze, "Fundamentals of the hydrodynamic mechanism of splitting in dispersion processes," *AIChE Journal*, vol. 1, no. 3, pp. 289–295, 1955.

[4] M. Pilch and C. Erdman, "Use of breakup time data and velocity history data to predict the maximum size of stable fragments for acceleration-induced breakup of a liquid drop," *International Journal of Multiphase Flow*, vol. 13, no. 6, pp. 741–757, 1987.

[5] R. Brodkey, *Formation of drops and bubbles*. Addison-Wesley, 1967.

[6] B. Gelfand, "Droplet breakup phenomena in flows with velocity lag," *Progress in Energy and Combustion Science*, vol. 22, no. 96, pp. 201–265, 1996.

[7] C. Schneider, W. Rasband, and K. Eliceiri, "NIH Image to ImageJ: 25 years of image analysis," *Nature Methods*, vol. 9, no. 7, pp. 671–675, 2012.